# Active and hibernating turbulence in drag-reducing plane Couette flows

Anselmo S. Pereira,[*] Gilmar Mompean,[†] and Laurent Thais[‡]

*Université de Lille 1, Sciences et Technologies, Polytech'Lille, and Laboratoire de Mécanique de Lille,
Cité Scientifique, 59655 Villeneuve d'Ascq, France*

Edson J. Soares[§]

*LabReo, Department of Mechanical Engineering, Universidade Federal do Espírito Santo,
Avenida Fernando Ferrari 514, Goiabeiras, 29075-910 Vitória, Espírito Santo, Brazil*

Roney L. Thompson[‖]

*COPPE, Department of Mechanical Engineering, Universidade Federal do Rio de Janeiro,
Centro de Tecnologia, Ilha do Fundo, 21945-970 Rio de Janeiro, Rio de Janeiro, Brazil*

(Received 23 January 2017; published 21 August 2017)

In this paper we analyze the active and hibernating turbulence in drag-reducing plane Couette flows using direct numerical simulations of the viscoelastic finitely extensible nonlinear elastic model with the Peterlin approximation fluids. The polymer-turbulence interactions are studied from an energetic standpoint for a range of Weissenberg numbers (from 2 up to 30), fixing the Reynolds number based on the plate velocities at 4000, the viscosity ratio at 0.9, and the maximum polymer molecule extensibility at 100. The qualitative picture that emerges from this investigation is a cyclic mechanism of energy exchange between the polymers and turbulence that drives the flow through an oscillatory behavior.

## I. INTRODUCTION

The reduction of the energy dissipation in turbulent flows by polymers has been widely analyzed over the years since the observations reported by Toms [1]. Despite the discrepancies between the most prominent theories concerning the nature of the polymer-induced drag reduction (DR) [2,3], it is well known that the phenomenon is bounded by two major laws: the Prandtl-Kármán law (when DR is null) and the so-called maximum drag reduction (MDR) or Virk's asymptote (when DR is maximum) [4]. The existence of the MDR's limit represents one of the most important issues in the DR context since changing the polymer concentration, the molecular weight, or even chemical characteristics of the additives produces no effect on this maximum drag-reduction level.

Recently, an important contribution to understanding the MDR's limit was given by Xi and Graham [5,6], who defined the MDR as a turbulent flow that fluctuates between two distinct states: active and hibernating. The former is related to the basic dynamical elements of Newtonian near-wall turbulence, exhibiting a higher drag. In contrast, during the latter state, the turbulent structures almost vanish, which reduces the drag. Xi and Graham [5,6], who performed direct numerical simulation (DNS) of turbulent plane Poiseuille flows of viscoelastic using the finitely extensible nonlinear elastic model with the Peterlin approximation (FENE-P fluids), pointed out that the flow oscillations between active and hibernating states, which also exist in the Newtonian turbulence, are accentuated by the presence of polymers.

---

[*]anselmo.pereira@polytech-lille.fr; anselmospereira@gmail.com

[†]gilmar.mompean@polytech-lille.fr

[‡]laurent.thais@polytech-lille.fr

[§]edson.soares@ufes.br

[‖]rthompson@mecanica.coppe.ufrj.br

In order to better understand the polymer-flow interactions in the MDR scenario, we investigate in the present paper the active and hibernating turbulences in drag-reducing plane Couette flows. The polymer effect on these two turbulent states are explored by taking into account a range of Weissenberg numbers, which provides drag-reduction levels from 11% up to 54%. Our DNSs are performed keeping the Reynolds number (based on the plate velocities), the viscosity ratio, and the maximum polymer molecule extensibility fixed. The results that emerge from energy transfer and spectral analyses reveal details concerning the effects of the polymers on the oscillatory behavior of turbulent viscoelastic flows through the active and hibernating states.

The organization of the paper is as follows. The description of the physical formulation and numerical method are presented in Sec. II. Our main results are discussed in Sec. III, where energy transfer and spectral analyses are conducted. Finally, a summary is given and conclusions are drawn in Sec. IV.

## II. PHYSICAL FORMULATION AND NUMERICAL METHOD

Following our previous work [7], turbulent plane Couette flows of incompressible dilute polymer solutions are considered. The flow is driven by both the top and the bottom plates, which have the same magnitude of velocity in the streamwise direction ($U_h$), but opposite senses. The streamwise direction is $x_1 = x$, the spanwise direction is $x_2 = y$, and the wall-normal direction is $x_3 = z$. The instantaneous velocity field in the respective directions is $(u_x, u_y, u_z) = (u, v, w)$ and it is solenoidal ($\nabla \cdot \boldsymbol{u} = 0$, where $\boldsymbol{u}$ denotes the velocity vector). Wall scaling is used and is based on zero-shear rate variables with the length and time scaled by $\nu_{\text{tot}}/u_\tau$ and $\nu_{\text{tot}}/u_\tau^2$, where $\nu_{\text{tot}} = \nu_N + \nu_{p0}$ is the total (solvent plus polymer) zero-shear viscosity and $u_\tau$ is the zero-shear friction velocity. Using this scaling, the dimensionless momentum equations are

$$\frac{\partial u_i^+}{\partial t^+} + u_j^+ \frac{\partial u_i^+}{\partial x_j^+} = -\frac{\partial p^+}{\partial x_i^+} + \beta_0 \frac{\partial^2 u_i^+}{\partial x_j^{+2}} + \frac{\partial \Xi_{ij}^+}{\partial x_j^+}, \tag{1}$$

where the plus superscript indicates the wall unit normalization, $p^+$ is the pressure, and $\beta_0$ is the ratio of the Newtonian solvent viscosity $\nu_N$ to the total zero-shear viscosity $\nu_{\text{tot}}$. The extra-stress tensor components are denoted by $\Xi_{ij}^+$. The formalism of Eq. (1) includes the assumption of a uniform polymer concentration in the dilute regime that is governed by the viscosity ratio $\beta_0$, where $\beta_0 = 1$ yields the limiting behavior of the Newtonian case. The extra-stress tensor components $\Xi_{ij}^+$ in Eq. (1) represent the polymer's contribution to the tension of the solution. This contribution is accounted for by a single-spring-dumbbell model. We employ here the FENE-P kinetic theory [8]. This model employs the phase-averaged conformation tensor $C_{ij} = \langle q_i q_j \rangle$, where the $q_i$ are the components of the end-to-end vector of each individual polymer molecule. The components of the extra-stress tensor $\boldsymbol{\Xi}^+$ are then $\Xi_{ij}^+ = \alpha_0[f\{\text{tr}(\boldsymbol{C})\}C_{ij} - \delta_{ij}]$ with $\alpha_0 = (1 - \beta_0)/\text{Wi}_{\tau 0}$, where $\text{Wi}_{\tau 0} = \lambda u_\tau^2 / \nu_{\text{tot}}$ is the friction Weissenberg number representing the ratio of the elastic relaxation time $\lambda$ to the viscous time scale. Additionally, $\delta_{ij}$ is the Kronecker delta and $f\{\text{tr}(\boldsymbol{C})\}$ is given by the Peterlin approximation $f\{\text{tr}(\boldsymbol{C})\} = \frac{L^2 - 3}{L^2 - \text{tr}(\boldsymbol{C})}$, where $L$ is the maximum polymer molecule extensibility and $\{\text{tr}(\cdot)\}$ represents the trace operator. This system of equations is closed with an evolution equation for the conformation tensor

$$\frac{DC_{ij}}{Dt^+} = (C_{ik}S_{kj}^+ + S_{ik}^+ C_{kj}) - (C_{ik}W_{kj}^+ + W_{ik}^+ C_{kj}) - \frac{f\{\text{tr}(\boldsymbol{C})\}C_{ij} - \delta_{ij}}{Wi_{\tau 0}}, \tag{2}$$

where $S_{ij}^+ = (\partial u_i^+/\partial x_j^+ + \partial u_j^+/\partial x_i^+)/2$ and $W_{ij}^+ = (\partial u_i^+/\partial x_j^+ - \partial u_j^+/\partial x_i^+)/2$ are, respectively, the terms of the rate-of-strain $\boldsymbol{S}^+$ and the rate-of-rotation $\boldsymbol{W}^+$ tensors.

We follow the same numerical method used by Pereira *et al.* [7] and all details of the scheme employed are given by Thais *et al.* [9]. We analyze here the interaction of the polymer molecules with the turbulence from the very beginning (when polymers are totally coiled) until the statistically-steady-state regime. The initial condition for the conformation tensor is the identity tensor, i.e., $\boldsymbol{C}(t = 0) = \boldsymbol{I}$. In addition, for each viscoelastic case, both the velocity and the pressure fields are

initially started from the same Newtonian fully developed turbulent flow. As a result of this method, the DR exhibits a marked transient behavior before achieving its asymptotic value, from a statistical point of view. We define the percentage of DR in time as

$$\mathrm{DR}(t) = \left( 1 - \frac{\langle \tau_w(t) \rangle}{\langle \tau_w(t=0) \rangle} \right) \times 100, \tag{3}$$

where $\langle \tau_w(t) \rangle$ is the area-averaged wall shear stress at a given instant $t$ and $\langle \tau_w(t=0) \rangle$ is the area-averaged wall shear stress at the very beginning of the simulation, when the polymers are in an isotropic configuration (coiled from an experimental point of view).

For the present study, we simulate the viscoelastic cases by fixing the Reynolds number based on the plate velocities $\mathrm{Re}_h = h U_h / \nu_{\mathrm{tot}}$ (where $h$ denotes the plane Couette half-width) at 4000, $\beta_0$ at 0.9, and $L$ at 100. Five cases are studied by setting the following Weissenberg numbers based on the plate velocities ($\mathrm{Wi}_h = \lambda U_h / h$): 2, 4.3, 10, 20, and 30. The respective asymptotic drag-reduction values $\mathrm{DR}_{\mathrm{asy}}$ are 11%, 33%, 50%, 53%, and 54%. Hence, both low drag reduction (LDR) (DR $<$ 40%) and high drag reduction (HDR) (DR $\geqslant$ 40%) scenarios are investigated. Finally, both the size of the domain ($L_x \times L_y \times L_z = 12\pi \times 4\pi \times 2$) and the number of mesh points ($N_x \times N_y \times N_z = 768 \times 512 \times 257$) are kept fixed for all cases, which leads to grid resolutions of $7.2 \leqslant \Delta x^+ \leqslant 9.5$, $3.6 \leqslant \Delta y^+ \leqslant 4.8$, and $0.2 \leqslant \Delta z^+ \leqslant 3.4$.

## III. RESULTS AND DISCUSSION

Our primary focus here is on the oscillatory behavior of the turbulent viscoelastic flow through the active and hibernating states, which is achieved by following the numerical method detailed by Pereira *et al.* [7]. Hence, at the very first instant of the simulation, the molecules are totally coiled, $\mathrm{tr}(\boldsymbol{C})/L^2 \approx 0$, the DR level is null, and the turbulent velocity field still exhibits a Newtonian-like nature. The flow is then characterized by the presence of a considerable number of turbulent structures, some of which are illustrated in Figs. 1(a) and 2(a) by using the $Q$ criterion [10] of flow classification[1] for the most elastic case ($\mathrm{Re}_h = 4000$, $\mathrm{Wi}_h = 30$, and $L = 100$). In Figs. 1 and 2, the vortical and extensional structures respectively described by $Q = 0.05$ and $Q = -0.05$ are colored from blue [$\mathrm{tr}(\boldsymbol{C})/L^2 = 0$] to red [$\mathrm{tr}(\boldsymbol{C})/L^2 = 1$], which indicates a distribution of the relative polymeric deformation over the domain. Since the development along time of the DR was already discussed in our previous work [7], we present here only a brief overview of the beginning of the phenomenon [shown in Figs. 1(a)–1(e) and 2(a)–2(e)] and we focus on the active and hibernating states illustrated in Figs. 1(f)–1(j) and 2(f)–2(j).

At the very beginning $t U_h / h = 0.3$ [Figs. 1(a) and 2(a)], the polymers are totally coiled and the turbulent structures appear with a Newtonian morphology [11]. The drag reduction at this instant is still negligible (DR $\approx$ 0%). The departure from this state develops toward highly negative values as the simulation evolves over time, moving from DR $\approx -6\%$ at $t U_h / h = 3$ [Figs. 1(b) and 2(b)] to its minimum value of DR $\approx -112\%$ at $t U_h / h = 9.6$ [Figs. 1(c) and 2(c)]. After that, the DR starts an increasing trajectory, reaching its positive peak of DR $\approx 77\%$ at $t U_h / h = 300$ [Figs. 1(d) and 2(d)] before it decreases towards an oscillatory state of a lower mean value (an asymptotic value from a statistical point of view). During this period, the molecules strongly interact with the flow, stretching [especially near the wall, as displayed in Figs. 1(c) and 2(c)] and partially suppressing the turbulent structures. At $t U_h / h \approx 525$ [Figs. 1(e) and 2(e)], DR starts to fluctuate around its time-averaged value $\mathrm{DR}_{\mathrm{asy}}$, indicating the beginning of the statistically-steady-state flow. A more detailed physical description of such developing time is presented by Pereira *et al.* [7].

––––––––

[1]The vortical (or elliptical) and extensional (or hyperbolic) structures are defined as the respective positive and negative values of the second invariant of the velocity gradient tensor, computed for incompressible flows by $Q = \frac{1}{2}(\|\boldsymbol{W}\|^2 - \|\boldsymbol{S}\|^2)$, where $\|\boldsymbol{W}\|$ and $\|\boldsymbol{S}\|$ denote the Euclidean norms of $\boldsymbol{W}$ and $\boldsymbol{S}$. The Euclidean norm of a generic second-order tensor $\boldsymbol{A}$ is $\|\boldsymbol{A}\| = \sqrt{\mathrm{tr}(\boldsymbol{A} \cdot \boldsymbol{A}^T)}$.
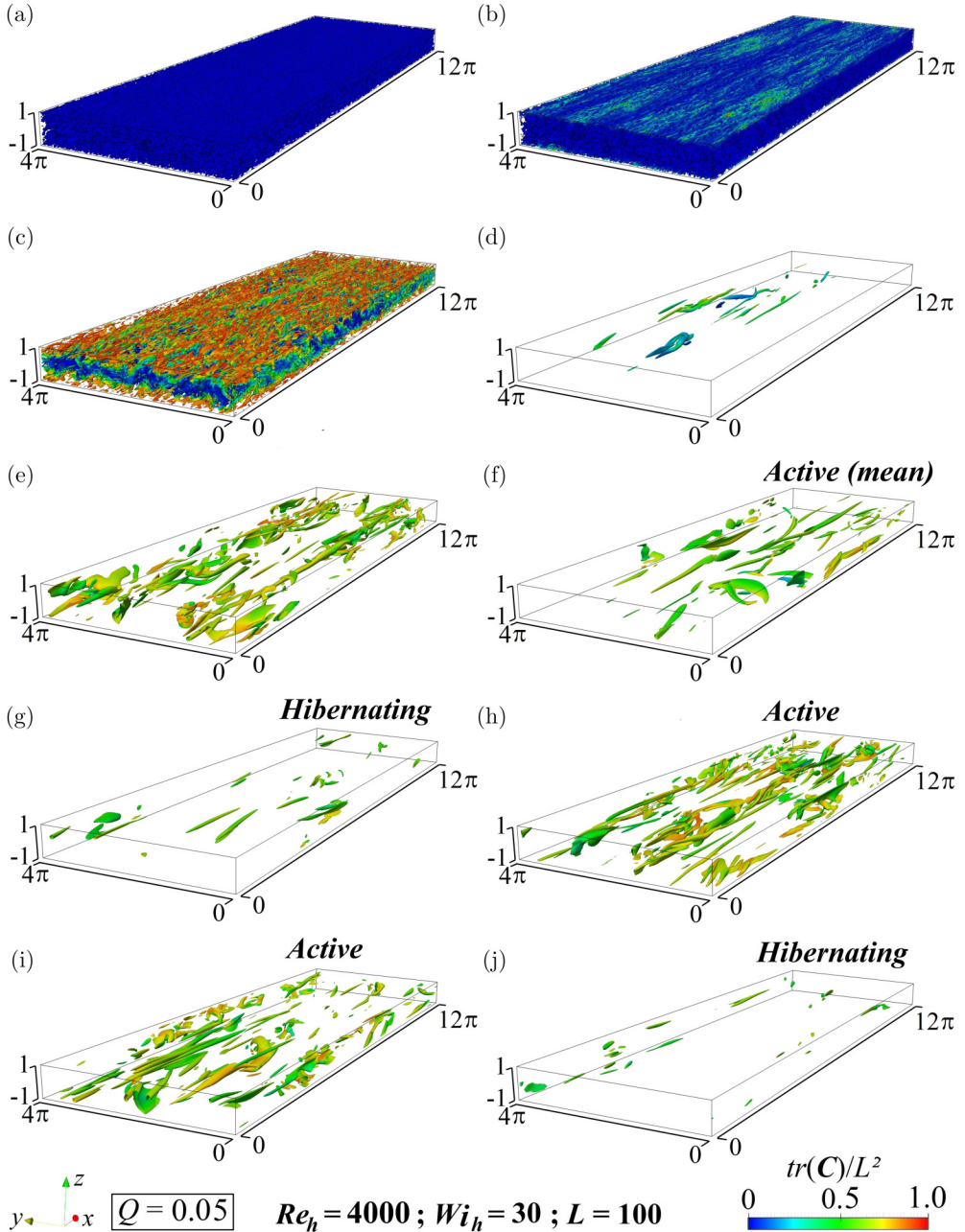
FIG. 1. Three-dimensional structures represent isosurfaces of vortical (or elliptical) regions defined as a positive value of the second invariant of the velocity gradient tensor $\nabla u$. The colors indicate the relative polymer stretching $\text{tr}(C)/L^2$. (a) $tU_h/h = 0.3$, $DR \approx 0\%$, (b) $tU_h/h = 3$, $DR \approx -6\%$, (c) $tU_h/h = 9.6$, $DR \approx -112\%$, (d) $tU_h/h = 300$, $DR \approx 77\%$, (e) $tU_h/h = 525$, $DR \approx 46\%$, (f) $tU_h/h = 640$, $DR \approx 54\%$, (g) $tU_h/h = 971$, $DR \approx 60\%$, (h) $tU_h/h = 1081$, $DR \approx 52\%$, (i) $tU_h/h = 1842$, $DR \approx 49\%$, and (j) $tU_h/h = 2063$, $DR \approx 63\%$.
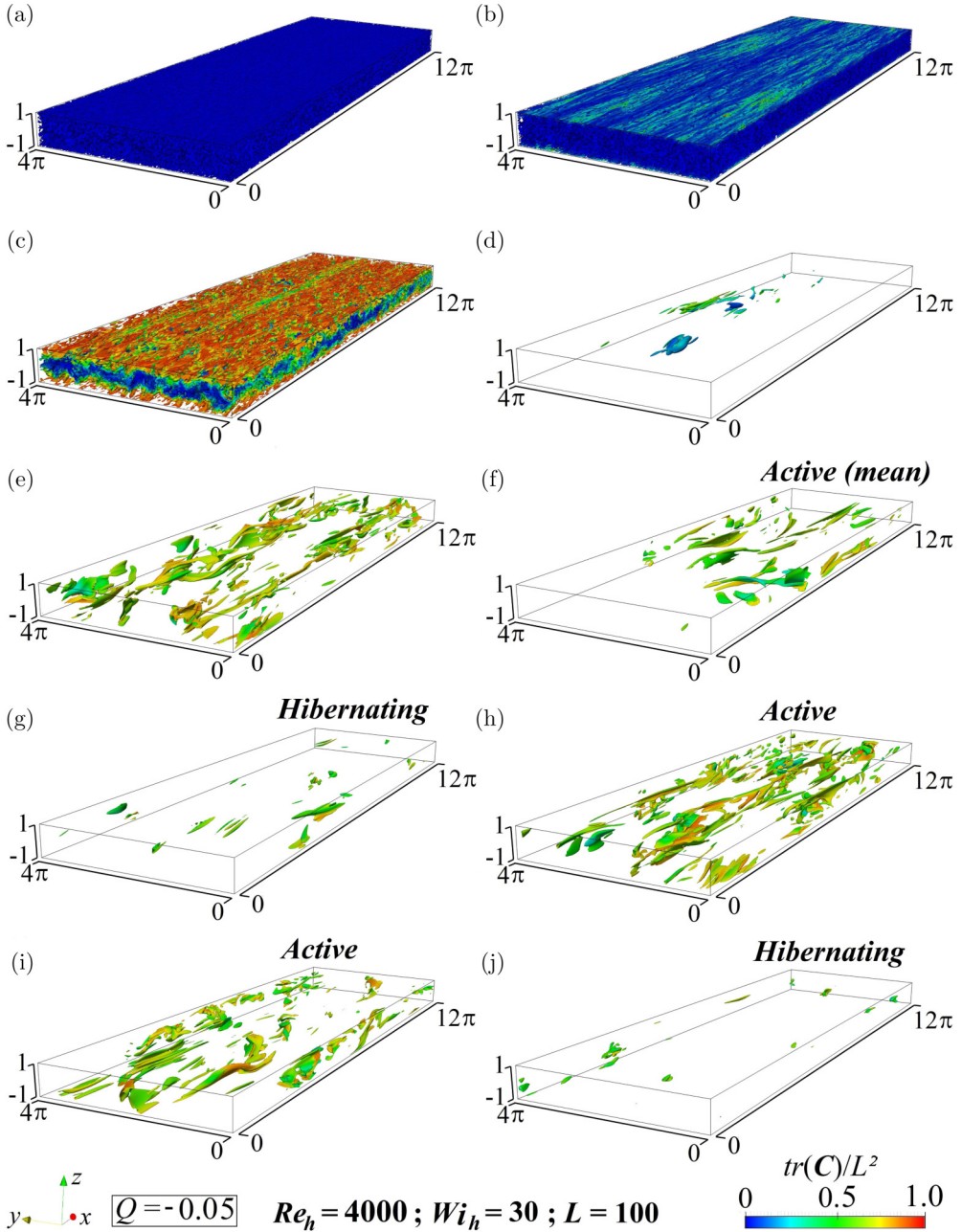
FIG. 2. Three-dimensional structures represent isosurfaces of extensional (or hyperbolic) regions defined as a positive value of the second invariant of the velocity gradient tensor $\nabla u$. The colors indicate the relative polymer stretching tr($C$)/$L^2$. (a) $tU_h/h = 0.3$, $DR \approx 0\%$, (b) $tU_h/h = 3$, $DR \approx -6\%$, (c) $tU_h/h = 9.6$, $DR \approx -112\%$, (d) $tU_h/h = 300$, $DR \approx 77\%$, (e) $tU_h/h = 525$, $DR \approx 46\%$, (f) $tU_h/h = 640$, $DR \approx 54\%$, (g) $tU_h/h = 971$, $DR \approx 60\%$, (h) $tU_h/h = 1081$, $DR \approx 52\%$, (i) $tU_h/h = 1842$, $DR \approx 49\%$, and (j) $tU_h/h = 2063$, $DR \approx 63\%$.
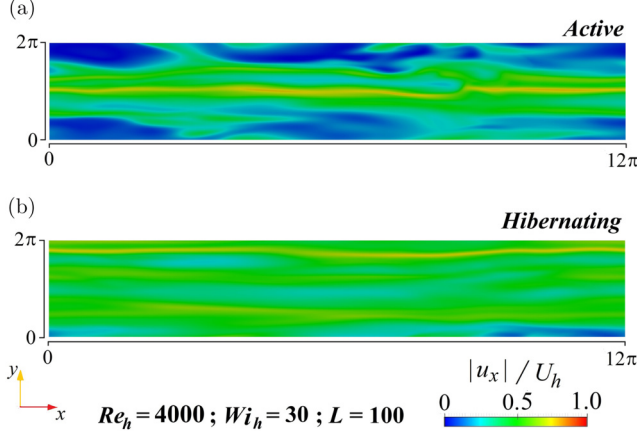
FIG. 3. Contours, in the $x$-$y$ center plane ($z = 0$), of the norm of the streamwise velocity made dimensionless by the plate velocities ($|u_x|/U_h$) at two dimensionless instants: (a) $tU_h/h = 1842$ (activation) and (b) $tU_h/h = 2063$ (hibernation).

At the dimensionless time $tU_h/h = 640$, the DR level is equal to 54%, which represents its asymptotic value $DR_{asy}$. Nevertheless, once the statistically steady state is reached ($tU_h/h > 525$), the turbulence starts to oscillate between periods of strong activation and hibernation. The differences between these two flow scenarios can be observed by comparing the turbulent structures pictured in Figs. 1(f) and 2(f) (our reference for the active state) with the others structures displayed in sequence. During highly active periods [Figs. 1(h), 1(i), 2(h), and 2(i)], the flow is dominated by the expected three-dimensional turbulent structures, the drag increases, and, in consequence, DR appears smaller than $DR_{asy}$. In contrast, within hibernating periods [Figs. 1(g), 1(j), 2(g), and 2(j)], the structures with $Q = \pm 0.05$ almost vanish, which is a distinct characteristic of the MDR. As a consequence, the drag decreases and DR assumes more pronounced values. At $tU_h/h = 2063$, for instance, DR approaches 63%, a value around 14% greater than that observed at $tU_h/h = 1842$. Contours, in the $x$-$y$ center plane ($z = 0$), of the norm of the streamwise velocity made dimensionless by the plate velocities ($|u_x|/U_h$) of these two dimensionless instants are illustrated in Fig. 3. At $tU_h/h = 1842$ [Fig. 3(a)], the turbulent activity is stronger and consequentially $|u_x|/U_h$ exhibits a shorter characteristic wavelength in the spanwise direction as well as a stronger dependence in the streamwise direction. In contrast, at $tU_h/h = 2063$ [Fig. 3(b)], low- and high-speed streaks have a weaker dependence in the $x$ direction. Hence, during the hibernation, much longer wavelength streaks are observed. As previously reported by Xi and Graham [5,6], extremely weak turbulent structures [Figs. 1(g), 1(f), 2(g), and 2(f)] and nearly streamwise-invariant streaks [Fig. 3(b)] are common characteristics between the MDR and the hibernating turbulence.

It is worth noting in Figs. 1 and 2 that the molecules are more stretched in the active state than in the hibernating one. This can be seen more clearly in Fig. 4, where the evolution of both the spatial average of the relative polymer stretching $\langle \mathrm{tr}(\boldsymbol{C}/L^2) \rangle_{xyz}$ (blue triangles) and the area-averaged wall shear stress dimensionalized by its asymptotic value $\langle \tau_w \rangle / \langle \tau_{w,asy} \rangle$ (red diamonds) are shown as functions of $tU_h/h$. Only the statistically steady state is considered ($500 < tU_h/h < 3000$). Our five cases are displayed: $Re_h = 4000$, $Wi_h = 30$, and $L = 100$ [Fig. 4(a)]; $Re_h = 4000$, $Wi_h = 20$, and $L = 100$ [Fig. 4(b)]; $Re_h = 4000$, $Wi_h = 10$, and $L = 100$ [Fig. 4(c)]; $Re_h = 4000$, $Wi_h = 4.3$, and $L = 100$ [Fig. 4(d)]; and $Re_h = 4000$, $Wi_h = 2$, and $L = 100$ [Fig. 4(e)]. The rectangular green boxes indicate the hibernating periods, which are identified by considering the criteria proposed by Xi and Graham [5]. The authors considered as hibernation the period of at least 50 s during which $\langle \tau_w \rangle / \langle \tau_{w,asy} \rangle$ drops below a cutoff value of 0.9, indicated by the black line in Figs. 4(a)–4(e). Clearly, the fraction of the total time of hibernation in our simulation $F_H$ (black asterisks) increases with $Wi_h$ as displayed in Fig. 4(f), which corroborates the results reported by Xi and Graham [5]. Additionally, a
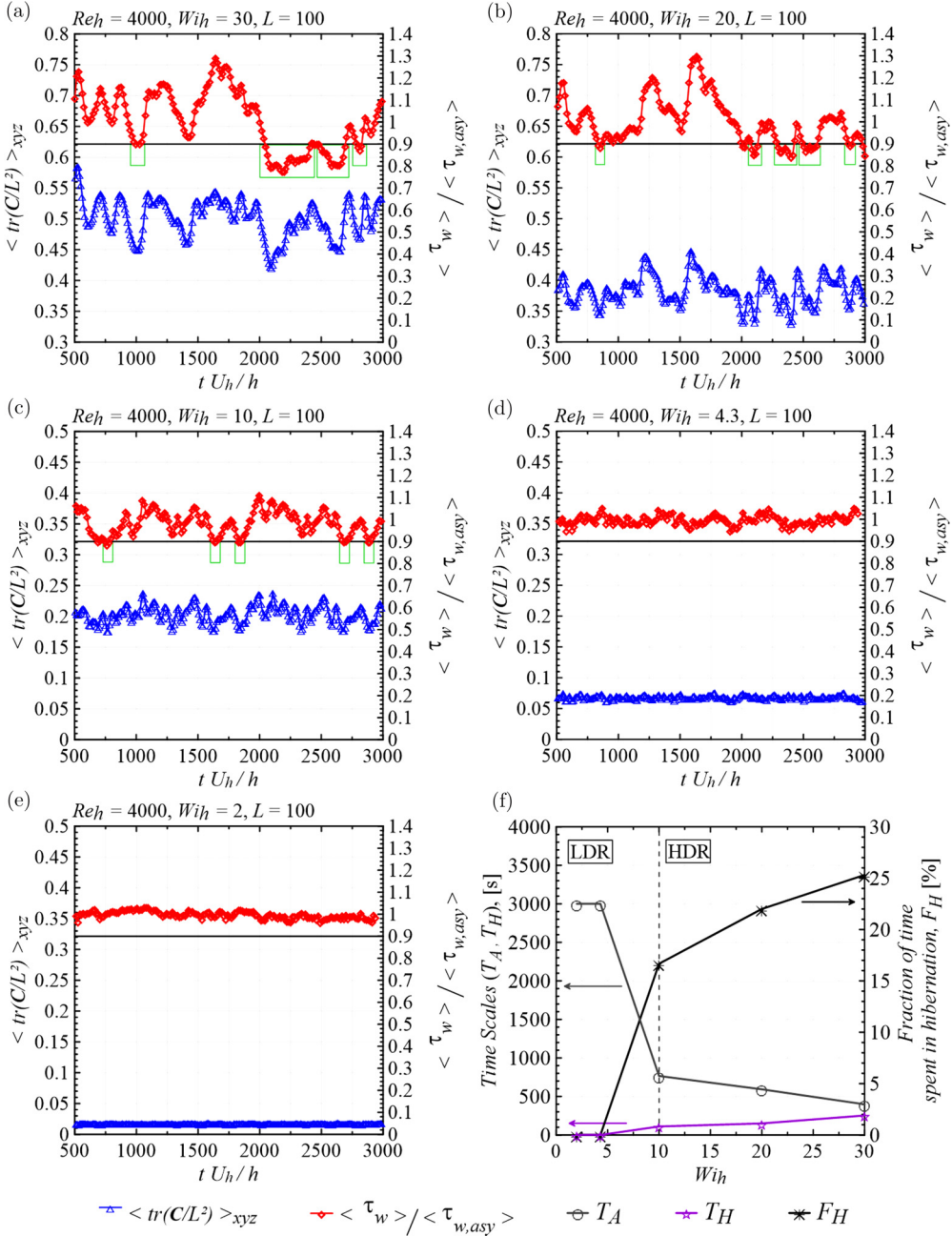
FIG. 4. (a)–(e) Evolution of the spatial average of the relative polymer stretching as a function of the dimensionless time $tU_h/h$ (blue triangles). The area-averaged wall shear stress is made dimensionless by its asymptotic value $\langle\tau_w\rangle/\langle\tau_{w,\text{asy}}\rangle$ as a function of the dimensionless time (red diamonds). (f) Time scales $T_A$ and $T_H$ and fraction of time spent in hibernation $F_H$.

maximum $F_H$ of 25% is observed, the same value found by Xi and Graham [5]. However, differently from the cited work, in the present paper, the hibernating turbulence is only observed in HDR scenarios ($10 \leqslant \text{Wi}_h \leqslant 30$) [Figs. 4(a)–4(c)]. In consequence, for the LDR cases [$\text{Wi}_h = 4.3$ and

$\mathrm{Wi}_h = 2$ in Figs. 4(d) and 4(e), respectively], the average duration of a hibernation period $T_H$ (purple stars) is null while the mean duration of active periods $T_A$ (gray open circles) becomes equal to the total physical time of the simulations ($T_A = 3000$ s). Furthermore, the reduction of stress also becomes less significant as $\mathrm{Wi}_h$ decreases. Finally, it is worth mentioning that the polymer stretching is in line with the wall shear stress, which means that the molecules are more stretched in the active periods.

The profile of the relative polymer extension is plotted in Fig. 5 (left column) together with the streamwise velocity (right column). Each point in this figure is an average in the $x$-$y$ plane along $z^+$. The channel half-width is divided into three distinct regions: I ($0 < z^+ < 5$), II ($5 < z^+ < 30$), and III ($z^+ > 30$). In order to compare our profiles with those available in the literature, the velocity of the bottom plate was subtracted from the velocity field, resulting in a relative streamwise component $u_{rx}$. Three cases with Re = 4000 and $L = 100$ are shown: $\mathrm{Wi}_h = 30$ [Figs. 5(a) and 5(b)], $\mathrm{Wi}_h = 10$ [Figs. 5(c) and 5(d)], and $\mathrm{Wi}_h = 4.3$ [Figs. 5(e) and 5(f)]. For each case, three different instants are considered: an instant for a moderately active state characterized by $\langle \tau_w \rangle / \langle \tau_{w,\mathrm{asy}} \rangle = 1$ and thus DR = $\mathrm{DR}_{\mathrm{asy}}$ (gray circles); an instant corresponding to a peak of $\langle \tau_w \rangle / \langle \tau_{w,\mathrm{asy}} \rangle$ (blue triangles), which indicates a strong active state for the HDR cases; and, finally, an instant relative to a valley of $\langle \tau_w \rangle / \langle \tau_{w,\mathrm{asy}} \rangle$ (red diamonds), which represents an intense hibernation for the HDR cases. It can be clearly observed that the differences between the active (Act) and the hibernating (Hib) states become more pronounced as $\mathrm{Wi}_h$ increases. In other words, the hibernation intensity is accentuated by the presence of polymers. For $\mathrm{Wi}_h = 4.3$, no hibernation is perceived and, in consequence, the curves practically collapse into a single one. The differences increase slightly for $\mathrm{Wi}_h = 10$ and become quite clear for $\mathrm{Wi}_h = 30$. At this level of elasticity, the hibernating velocity profile (red diamonds) approaches the Virk asymptote (red dash-dotted line). Moreover, the $u_{rx}$ profile corresponding to the most active case (blue diamond) is markedly below the curve that represents the time-averaged asymptotic profile (gray circles), getting close to the log-law profile represented by the gray dotted line. Concerning the most elastic case, it is also important to mention that the polymers appear more extended in the active periods. In contrast, in the hibernating periods, the molecules are in their least stretched configuration. Such an observation is similar to the phenomenon reported by Xi and Graham [5,6] for turbulent plane Poiseuille flows.

Differences between the active and the hibernating turbulence can also be perceived by analyzing the normal and the cross components of the instantaneous Reynolds stress tensor displayed in Figs. 6(a)–6(d). Average values in the $x$-$y$ plane $\langle u_i'^+ u_j'^+ \rangle$ are evaluated as a function of $z^+$ at three dimensionless instants for the most elastic case ($\mathrm{Re}_h = 4000$, $\mathrm{Wi}_h = 30$, and $L = 100$): $t U_h / h = 640$ (moderately active state, gray circles), $t U_h / h = 1842$ (a peak of the active state, blue triangles), and $t U_h / h = 2063$ (a valley of hibernation, red diamonds). A comparison of the Reynolds stresses during the moderately active state ($\langle \tau_w \rangle / \langle \tau_{w,\mathrm{asy}} \rangle = 1$) and the peak of activation reveals that these terms increase during strong active periods. Interestingly, a stronger tensor anisotropy is observed within hibernating periods. The streamwise Reynolds stress component [red diamonds in Fig. 6(a)] becomes even more pronounced, while the other normal terms [red diamonds in Figs. 6(a)–6(c)] decrease compared with the active states. The hibernating Reynolds shear stress [red diamonds in Fig. 6(d)] then assumes a particular profile, fitting the moderately active curve [gray circles in Fig. 6(d)] within regions I and II, and becoming the larger shear stress term close to the channel center ($z^+ > 100$).

In an attempt to further understand the role played by the active and hibernating turbulences in drag-reducing flows, we conduct an analysis from the energy transfer and the spectral perspectives, which are displayed in Figs. 7–9. Figure 7 shows the average values in the $x$-$y$ plane of the instantaneous kinetic energy terms obtained from the work equation [7]

$$\underbrace{\left[ \frac{1}{2} \frac{\partial (u_x^{+2})}{\partial t^+} \right]}_{T_x^+} = \underbrace{\left[ -u_x^+ \frac{\partial (u_x^+ u_j^+)}{\partial x_j^+} \right]}_{A_x^+} + \underbrace{\left[ -u_x^+ \frac{\partial p^+}{\partial x^+} \right]}_{P_x^+} + \underbrace{\left[ (\beta_0) u_x^+ \frac{\partial^2 u_x^+}{\partial x_j^{+2}} \right]}_{V_x^+} + \underbrace{\left[ u_x^+ \frac{\partial \Xi_{xj}^+}{\partial x_j^+} \right]}_{E_x^+}, \qquad (4)$$
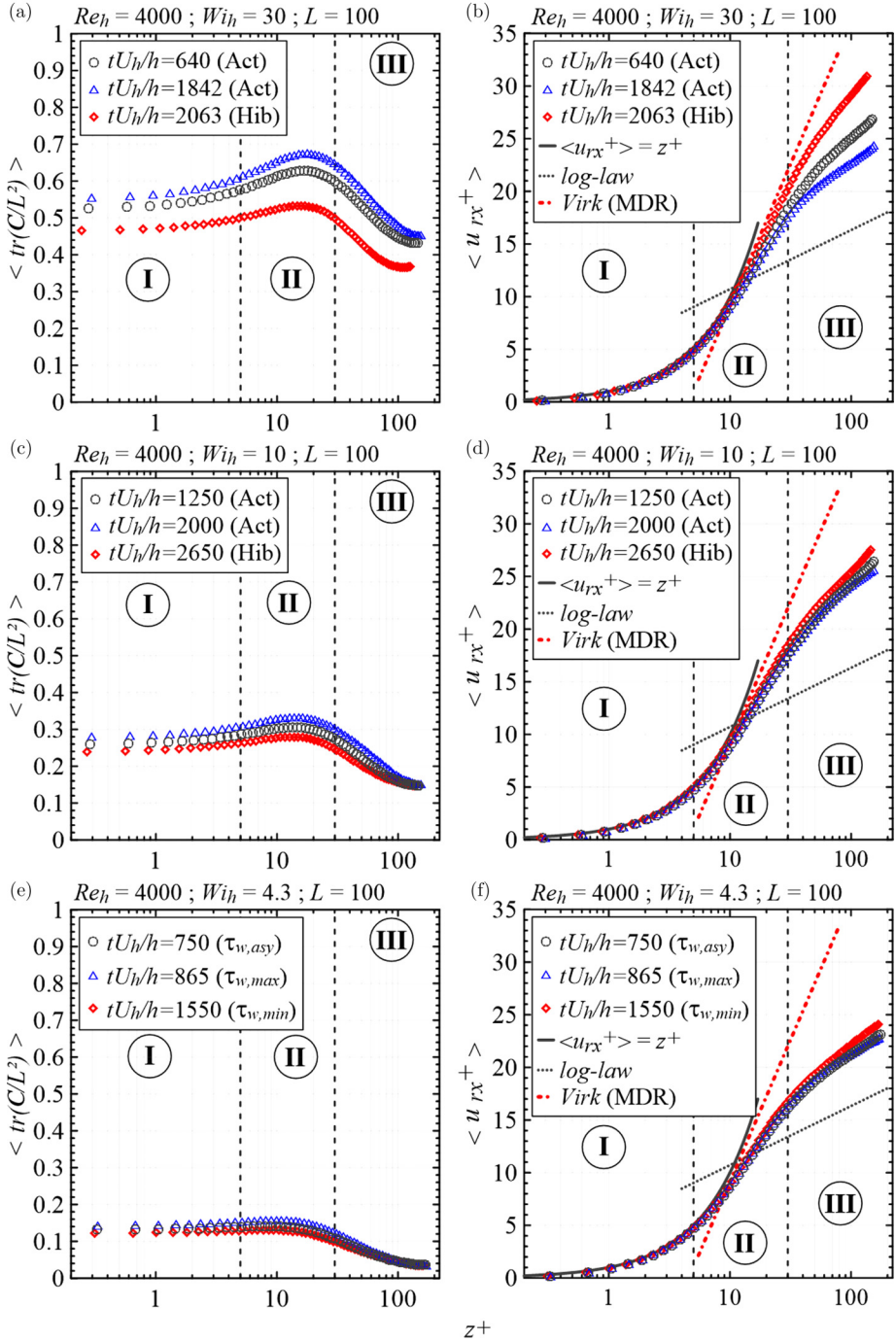
FIG. 5. The left column shows average values in the $x$-$y$ plane of the relative polymer stretching $\langle \mathrm{tr}(\boldsymbol{C})/L^2 \rangle$ as a function of the dimensionless wall distance. The right column shows average values in the $x$-$y$ plane of the streamwise relative velocity $\langle u_{rx}^+ \rangle$ as a function of the dimensionless wall distance. Three FENE-P turbulent flows are analyzed: (a) and (b) $\mathrm{Re}_h = 4000$, $\mathrm{Wi}_h = 30$, and $L = 100$; (c) and (d) $\mathrm{Re}_h = 4000$, $\mathrm{Wi}_h = 10$, and $L = 100$; and (e) and (f) $\mathrm{Re}_h = 3000$, $\mathrm{Wi}_h = 4.3$ and $L = 100$. For each viscoelastic flow, $\langle \mathrm{tr}(\boldsymbol{C})/L^2 \rangle$ and $\langle u_{rx}^+ \rangle$ are analyzed at three dimensionless instants $t U_h / h$.
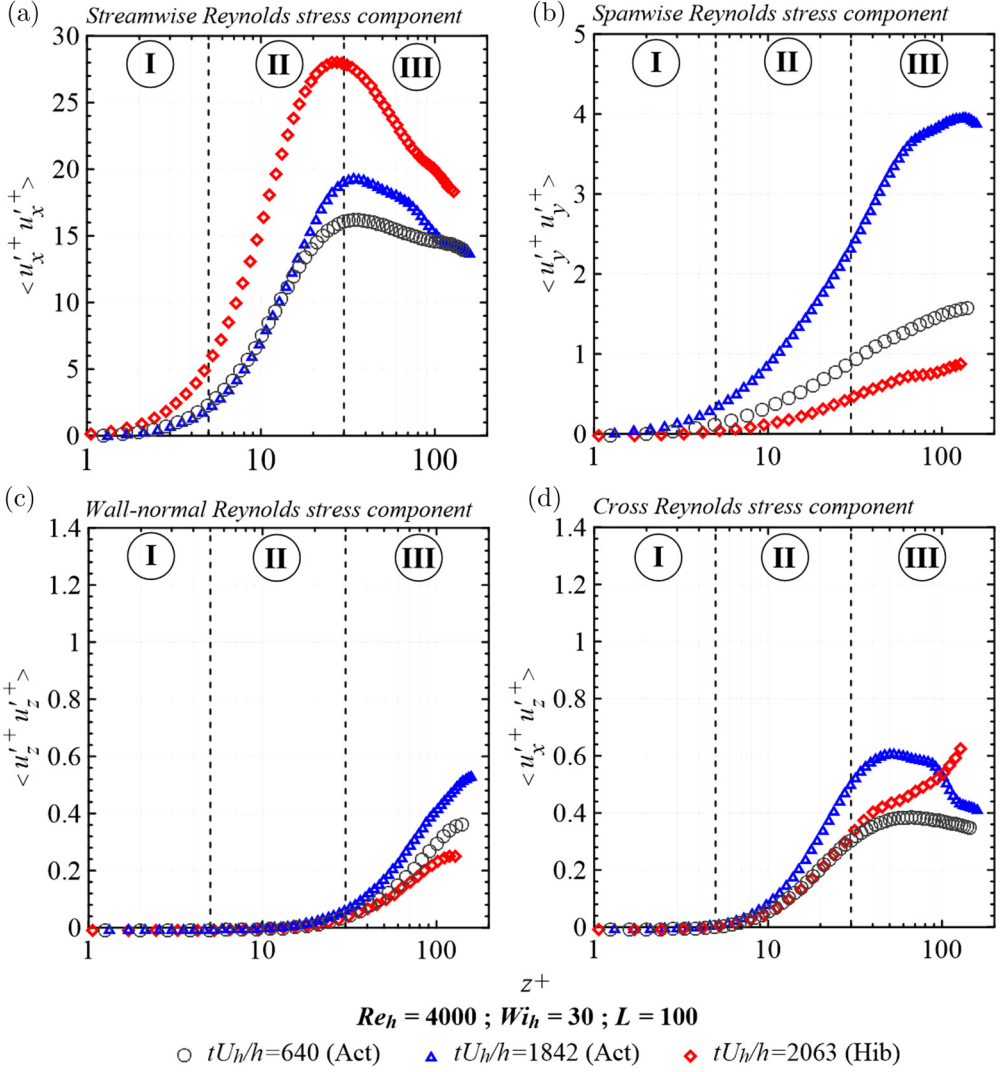
FIG. 6. (a)–(c) Normal and (d) cross components of the instantaneous Reynolds stress tensor. Average values in the $x$-$y$ plane, $\langle u_i'^{+} u_j'^{+} \rangle$, are evaluated as a function of $z^{+}$ at three dimensionless instants for the most elastic case: $tU_h/h = 640$ (moderately active state) (gray circles), $tU_h/h = 1842$ (a peak of the active state) (blue triangles), and $tU_h/h = 2063$ (a valley of hibernation) (red diamonds).

where the instantaneous polymer work term $E_x^{+}$ indicates the amount of energy stored ($E_x^{+} < 0$) or released ($E_x^{+} > 0$) by the polymers from the velocity field in the streamwise direction $u_x^{+}$. The complementary work terms denote the advection by $A_x^{+}$, the pressure redistribution by $P_x^{+}$, and the viscous stress by $V_x^{+}$. The sum $A_x^{+} + P_x^{+} + V_x^{+}$ is referred to as the Newtonian work $N_x^{+}$ and $T_x^{+}$ is the local time derivative term. The $x$-$y$ plane averages of these terms are plotted as a function of $z^{+}$. The profiles are evaluated at $tU_h/h = 1842$ (a peak of the active state) [Fig. 7(a)] and $tU_h/h = 2063$ (a valley of hibernation) [Fig. 7(b)] for the most elastic case. In fact, a careful analysis of the energy exchange for the drag-reducing flow between parallel plates was reported in Pereira *et al.* [7]. In the present paper it is worth noting the main difference between each term of the kinetic energy in the active and hibernating states, displayed in Figs. 7(a) and 7(b). The main difference refers to the polymeric (blue pluses) and the viscous (green squares) works within the viscous sublayer (region I).
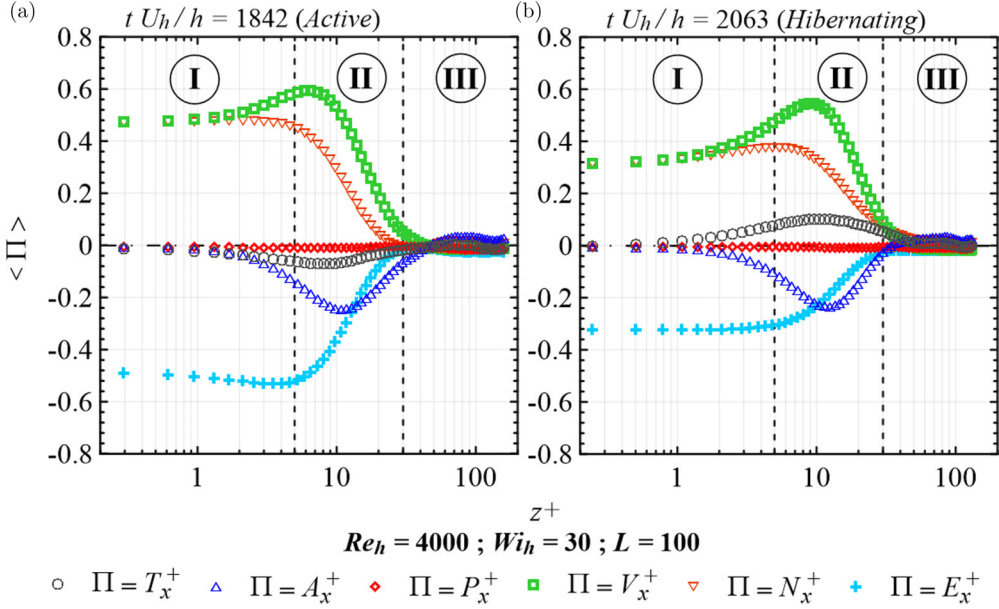
FIG. 7. Average values in the $x$-$y$ plane of the streamwise total kinetic energy transfer against the dimensionless wall distance for the most elastic case. Two dimensionless instants $tU_h/h$ are analyzed.

The energy stored by the polymers near the wall is clearly less pronounced during the hibernating state. This term is balanced by the viscous work, which also decreases in the hibernation.

There are striking differences between the active and hibernating states that appear in Fig. 8, where the $x$-$y$ averages of fluctuating work terms are displayed across the channel half-width for
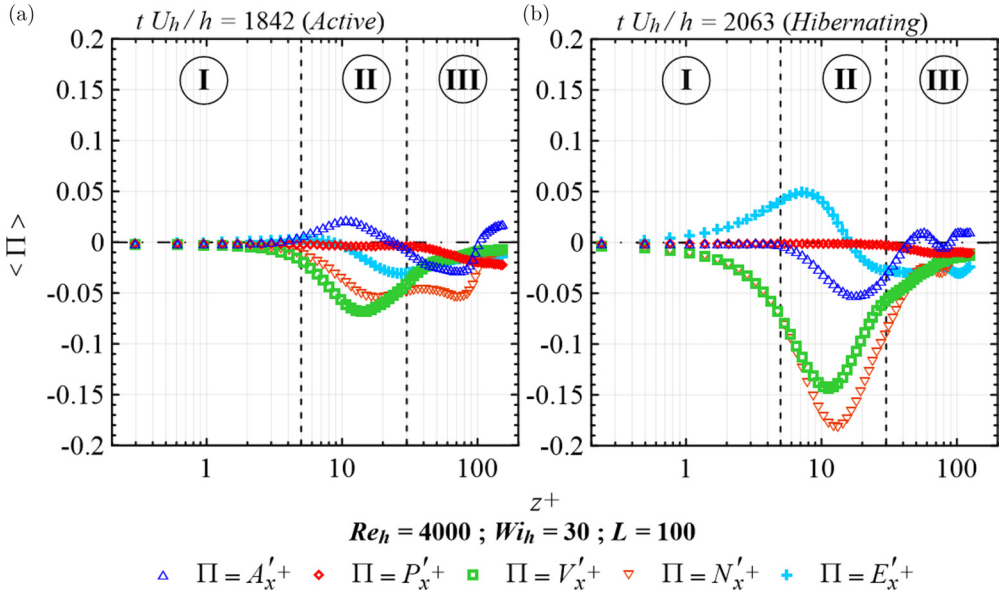


FIG. 8. Average values in the $x$-$y$ plane of the streamwise fluctuating kinetic energy transfer against the dimensionless wall distance for the most elastic case. Two dimensionless instants $tU_h/h$ are analyzed.
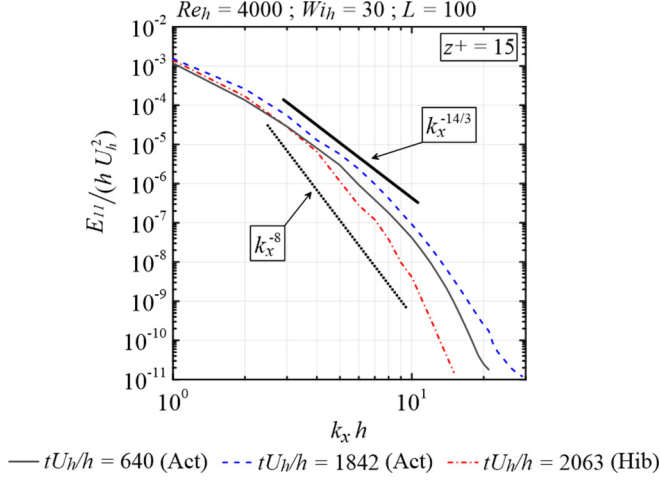
FIG. 9. Power spectral densities of the streamwise velocity component at the wall-normal position $z^+ = 15$ for the most elastic case. Three dimensionless instants $t U_h / h$ are analyzed.

the most elastic case. These energy terms are that exclusively related to the fluctuating fields that appear on the right-hand side of the streamwise work fluctuation equation, which in turn is obtained by decomposing the variables of the streamwise momentum equation into mean flow ($\bar{U}_x^+$, $\bar{p}^+$, and $\bar{\Xi}_{xj}^+$) and fluctuations ($u_x'^+$, $p'^+$, and $\Xi_{xj}'^+$), and then multiplying the resulting equation by the streamwise velocity fluctuation $u_x'^+$ (a detailed deduction of the work equations is provided in [12]). The work terms exclusively linked with the fluctuating fields are then $E_x'^+ = (u_x'^+ \frac{\partial \Xi_{xj}'^+}{\partial x_j^+})$, $A_x'^+ = [-u_x'^+ \frac{\partial (u_x'^+ u_j'^+)}{\partial x_j^+}]$, $P_x'^+ = (-u_x'^+ \frac{\partial p'^+}{\partial x^+})$, and $V_x'^+ = [(\beta_0) u_x'^+ \frac{\partial^2 u_x'^+}{\partial x_j^{+2}}]$. The instantaneous polymer work term $E_x'^+$ indicates the amount of energy stored ($E_x'^+ < 0$) or released ($E_x'^+ > 0$) by the polymers from the fluctuating velocity field in the streamwise direction $u_x'^+$ (the fluctuations are denoted by the prime superscript). The supplementary fluctuating work terms denote the advection by $A_x'^+$, the pressure redistribution by $P_x'^+$, and the viscous stress by $V_x'^+$. The sum $A_x'^+ + P_x'^+ + V_x'^+$ is referred to as the Newtonian fluctuating work $N_x'^+$. Following the profiles shown in Fig. 8, it can be clearly seen that, when the flow state changes from the active [Fig. 8(a)] to the hibernating one [Fig. 8(b)], the magnitudes of both the advection ($|A_x'^+|$) and the pressure ($|P_x'^+|$) work fluctuations decrease far from the wall (region III). However, $|A_x'^+|$ increases within the region II. The same tendency is observed for $|V_x'^+|$. It is worth noting that, in the active state, the molecules located in the regions II and III store energy from the fluctuating velocity field ($E_x'^+ < 0$). However, this scenario considerably changes during the hibernation since significant positive values of $E_x'^+$ are perceived within the region II, which indicates a release of energy by the polymers in the streamwise fluctuating velocity field. More specifically, the polymer elasticity moves the turbulent kinetic energy from the transverse components ($y$ and $z$) to the streamwise velocity fluctuation in the near-wall region, which is consistent with the elastic theory described by Tabor and de Gennes [3]. Hence, we can conclude that, especially during the hibernating state, the polymers considerably favor the increase of the streamwise turbulent kinetic energy in region II. In other words, the turbulence tends to be reactivated by the polymers, which, finally, increases $|N_x'^+|$, as indicated by the orange inverted triangles in Fig. 8(b). This is rather in line with the description provided by Dubief *et al.* [13], who numerically showed that, in the absence of an elastic term in the streamwise momentum equation, the flow laminarizes at high $Wi_h$, thereby indicating that the near-wall injection of elastic energy

into the streamwise velocity component plays a cardinal role in the sustainability of HDR scenarios. The polymer-turbulence exchanges of energy in the hibernating state may provide a reasonable explanation for the MDR's limit, as previously speculated by Dubief *et al.* [14]. Xi and Graham [5] argue that the MDR scenario is a state in which hibernating turbulence is the norm, with active turbulence arising intermittently.

Finally, Fig. 9 shows the longitudinal one-dimensional spectra of the turbulent kinetic energy $E_{11}/hU_h^2$ at $z^+ = 15$ for the most elastic case. Around this point, $|N_x'^+|$ is maximum for both the active and hibernating states (see Fig. 8). For the former state, illustrated by the gray solid line and the blue dashed line, a range of wave numbers $3 \leqslant k_x \leqslant 9$ exhibits the typical power-law decay related to drag-reducing flows $k_x^{-14/3}$ (black solid line) [15]. However, such a decay is modified in the hibernating period, moving from $k_x^{-14/3}$ towards $k_x^{-8}$ (black dotted line). Consequently, the large-wave-number structures ($k_x > 15$) are strongly suppressed. In contrast, within very small wave numbers, no significant changes in $E_{11}/hU_h^2$ are perceived by comparing the three curves plotted in Fig. 9. Hence, we can conclude that the oscillatory behavior of the turbulence between the active and hibernating states affects basically the small-scale structures (high frequencies), which in turn tend to be suppressed before the hibernation while the large structures (low frequency) are preserved. Finally, it is important to emphasize that the profiles of $E_{11}/hU_h^2$ collapse into a single one at $\mathrm{Wi}_h = 4.3$ and $\mathrm{Wi}_h = 2$ (not shown, for brevity).

## IV. CONCLUSION

Direct numerical simulations of FENE-P fluids were used to analyze the active and hibernating turbulence states in drag-reducing plane Couette flows. Five viscoelastic flows were examined, keeping the Reynolds number $\mathrm{Re}_h = 4000$, the viscosity ratio $\beta_0 = 0.9$, and the maximum polymer molecule extensibility $L = 100$ fixed. A large range of Weissenberg numbers based on the plate velocities was explored ($2 \leqslant \mathrm{Wi}_h \leqslant 30$), which provided asymptotic drag-reduction levels $\mathrm{DR}_{\mathrm{asy}}$ from 11% (LDR) up to 54% (HDR).

Graham and co-workers [5,6,16] have demonstrated that the oscillation between the active and the hibernating states is present in Newtonian flows and is accentuated by the polymers. In the present work, the hibernation was only detected in HDR scenarios ($10 \leqslant \mathrm{Wi}_h \leqslant 30$). This seems to indicate that the hibernation could be attenuated by the increase of the Reynolds number, a possibility that needs further investigation.

Concerning the drag-reducing flows with oscillations between active and hibernating states, the qualitative picture that emerges from our energy transfer and spectral analyses is a cycle that begins when the polymer-flow interactions in the active turbulence state favor the extension of the molecules. In their stretching process, polymers reduce the mean fluid velocity and partially suppress the turbulent structures (the small-scale ones), driving the flow towards a very weak turbulent hibernating state in which the polymers tend to relax. Hence, their level of stretching decreases while a significant amount of energy is released by the polymers into the flow, increasing its mean velocity towards the MDR asymptote. Additionally, polymers also directly inject energy into the fluctuating velocity field, favoring the reactivation of turbulence. Finally, the active turbulence stretches the molecules again, reinitiating the cycle.

[1] B. A. Toms, *Proceedings of the International Congress of Rheology* (North-Holland, Amsterdam, 1948), Sec. II, p. 135.

[2] J. L. Lumley, Drag reduction by additives, Annu. Rev. Fluid Mech. **11**, 367 (1969).

[3] M. Tabor and P. G. de Gennes, A cascade theory of drag reduction, Europhys. Lett. **2**, 519 (1986).

[4] P. S. Virk, E. W. Merrill, H. S. Mickley, K. A. Smith, and E. L. Mollo-Christensen, The Toms phenomenon: Turbulent pipe flow of dilute polymer solutions, J. Fluid Mech. **30**, 305 (1967).

[5] L. Xi and M. D. Graham, Active and Hibernating Turbulence in Minimal Channel Flow of Newtonian and Polymeric Fluids, Phys. Rev. Lett. **104**, 218301 (2010).

[6] L. Xi and M. D. Graham, Dynamics on the Laminar-Turbulent Boundary and the Origin of the Maximum Drag Reduction Asymptote, Phys. Rev. Lett. **108**, 028301 (2012).

[7] A. S. Pereira, G. Mompean, L. Thais, and E. J. Soares, Transient aspects of drag reducing plane Couette flows, J. Non-Newtonian Fluid Mech. **241**, 60 (2017).

[8] R. Bird, R. Armstrong, and O. Hassager, *Dynamics of Polymeric Liquids, Volume 2: Kinetic Theory*, 2nd ed. (Wiley-Interscience, New York, 1987).

[9] L. Thais, A. Tejada-Martinez, T. B. Gatski, and G. Mompean, A massively parallel hybrid scheme for direct numerical simulation of turbulent viscoelastic channel flow, Comput. Fluids **43**, 134 (2011).

[10] J. C. R. Hunt, A. A. Wray, and P. Moin, Eddies, stream, and convergence zones in turbulent flows, Center for Turbulence Research, Proceedings of Summer Program Report No. CTR-S88, Stanford University (1988), p. 193.

[11] R. J. Adrian, Hairpin vortex organization in wall turbulence, Phys. Fluids **19**, 041301 (2007).

[12] A. S. Pereira, G. Mompean, L. Thais, and R. L. Thompson, Statistics and tensor analysis of polymer coil-stretch mechanism in turbulent drag reducing channel flow, J. Fluid Mech. **824**, 135 (2017).

[13] Y. Dubief, V. E. Terrapon, C. M. White, E. S. G. Shaqfeh, P. Moin, and S. K. Lele, New answers on the interaction between polymers and vortices in turbulent flows, Flow, Turbul. Combust. **74**, 311 (2005).

[14] Y. Dubief, C. M. White, V. E. Terrapon, E. S. G. Shaqfeh, P. Moin, and S. K. Lele, On the coherent drag-reducing and turbulence-enhancing behavior of polymers in wall flows, J. Fluid Mech. **514**, 271 (2004).

[15] L. Thais, T. B. Gatski, and G. Mompean, Spectral analysis of turbulent viscoelastic and Newtonian channel flows, J. Non-Newtonian Fluid Mech. **200**, 165 (2013).

[16] M. D. Graham, Drag reduction and the dynamics of turbulence in simple and complex fluids, Phys. Fluids **26**, 101301 (2014).